Scientific paper

Phase Equilibria in the Ag_2Te-PbTe-Sb_2Te_3 System and Thermodynamic Properties of the $(2PbTe)_{1-x}(AgSbTe_2)_x$ Solid Solutions

Leyla Farhad Mashadiyeva,[1] Shabnam Hamlet Mansimova,[2] Dunya Mahammad Babanly,[1,3] Yusif Amirali Yusibov,[4] Dilqam Babir Tagiyev[1] and Mahammad Baba Babanly[1,2,*]

[1] *Institute of Catalysis and Inorganic Chemistry, Azerbaijan National Academy of Science, Baku, Azerbaijan*

[2] *Baku State University, Chemistry Department, Baku, Azerbaijan*

[3] *Azerbaijan State Oil and Industry University, Baku, Azerbaijan*

[4] *Ganja State University, Chemistry Department, Ganja, Azerbaijan*

* *Corresponding author: E-mail: babanlymb@gmail.com*

Received: 13-29-2019

Abstract

Phase equilibria in the Ag_2Te-PbTe-Sb_2Te_3 system were experimentally investigated by means of differential thermal analysis, powder X-ray diffraction techniques and electromotive force (EMF) measurement method. A liquidus surface projection of the system, 750 K and 300 K isothermal sections, as well as five vertical sections of the phase diagram, were constructed. The primary crystallization fields of phases and homogeneity range of phases were also determined. The character and temperature of the various nonvariant and monovariant equilibria were identified. The studied system is characterized by the formation of a wide continuous band of a high-temperature cubic structured solid solution (β-phase) between PbTe and $Ag_{1-x}Sb_{1+x}Te_{2+x}$ intermediate phase. The partial molar thermodynamic functions of lead telluride in alloys and standard integral thermodynamic functions of the β-solid solutions along the 2PbTe-"$AgSbTe_2$" section were calculated based on the EMF measurements results.

Keywords: Ag-Sb-Pb-Te system; silver telluride; lead telluride; antimony telluride; phase equilibria; solid solution; thermodynamic functions.

1. Introduction

Complex silver-containing chalcogenides are among the advanced functional materials.[1–3] Thanks to the mobility of silver ions, these phases have mixed ion-electron conductivity and can be widely used in semiconductors, electrochemical energy storage materials, electrodes of fuel cells and batteries, etc.[4,5]

Alloys formed in Ag_2X-$A^{IV}X$-$B^V{}_2X_3$ systems (where A^{IV} = Ge, Sn, Pb; B^V = Sb, Bi; X = S, Se, Te) are good thermoelectric materials with a high thermoelectric figure of merit ZT.[6–10] Besides, phases $A^{IV}B^V{}_2X_4$, $A^{IV}B^V{}_4X_7$, etc. which are formed on the boundary quasi-binary systems of the Ag_2X-$A^{IV}X$-$B^V{}_2X_3$ systems possess topological surface states and can be used in spintronics and quantum computing.[11–14] Great interest is complex telluride phases formed in these systems with excellent thermoelectric properties, such as Ge-Sb-Ag-Te (named as TAGS) and Pb-Sb-Ag-Te (denoted as LAST).[15–19] It is known that the development of new multicomponent materials is based on data on the phase equilibria of the corresponding systems and thermodynamic properties of phases formed in them.[20–24]

Herein, we present the phase relationships in the Ag_2Te-PbTe-Sb_2Te_3 system over the entire concentration range. Also, we report the thermodynamic properties of the $(2PbTe)_{1-x}(AgSbTe_2)_x$ solid solution formed in the system. Earlier we report the self-consistent phase equilibria description and thermodynamic study result in such silver-based multi-component telluride systems

Ag_2Te-PbTe-Bi_2Te_3,[25] Ag_2Te-SnTe-Bi_2Te_3,[26] and Ag_2Te-SnTe-Sb_2Te_3.[27,28] In all these studied systems, high-temperature solid solutions with a cubic structure along the $A^{IV}Te$-$AgB^{V}_2Te_3$ section are formed.

2. Literature Review

2. 1. Starting Compounds

The starting binary compounds of the Ag_2Te-PbTe-Sb_2Te_3 system are well known. Ag_2Te melts congruently at 1233 K and has three polymorph modifications.[29] Its room-temperature modification (RT-Ag_2Te) crystallizes in the monoclinic system ($P2_1/c$ space group; lattice parameters: a = 0.809 nm; b = 0.448 nm; c = 0.896; β = 112.55°) and remains stable up to 378 K with tellurium excess and up to 418 K with silver excess.[30] Intermediate-temperature modification (IT-Ag_2Te) crystallizes in the face-centered cubic system ($Fm\bar{3}m$ space group; a = 0.6648 nm,[31]) transforms into high temperature body-centered cubic form (HT-Ag_2Te; $Im\bar{3}m$ space group; a = 0.529 nm,[32]) at 1075 K. PbTe melts congruently at 1197 K,[29] and crystallizes in in the $Fm\bar{3}m$ face-centered cubic crystal structure with cell parameter; a = 6.6461(3) nm.[33] Sb_2Te_3 melts congruently at 893 K,[29] and crystallizes in the rhombohedral tetradymite type of structure ($R\bar{3}m$ space group) with parameters: a = 0.4264 nm; c = 3.0458 nm.[34]

2. 2. Boundary Quasi-Binary Systems

The boundary quasi-binary systems of the Ag_2Te-PbTe-Sb_2Te_3 system were studied well.

The Ag_2Te-PbTe system has a T-x diagram of eutectic type with limited mutual solubility of the components.[35–37] The eutectic has the composition 38 mol % PbTe and crystallizes at 967 K,[36] (35 mol % PbTe and 973 K,[35]). The solubility of the starting components in each other is 12–15% at the eutectic temperature.[37]

Phase diagrams of the Ag_2Te-Sb_2Te_3 pseudobinary system were elaborated separately in.[38,39] A previously reported in,[40] phase with the nominal composition of Ag_2SbTe_2 does not exist. In fact, the only ternary intermediate phase $Ag_{1-x}Sb_{1+x}Te_{2+x}$ with variable composition ($0.08 < x < 0.41$,[38]), which crystallizes in the NaCl structure type ($Fm\bar{3}m$ space group; a = 0.6078 nm,[38]) is thermodynamically stable. However, earlier reports differ about the temperature and compositional region of this phase.[38,39] Further investigations of the Ag-Sb-Te ternary system confirmed that this phase is only stable in a limited temperature range (633 K < T < 847 K) and it decomposes into solid solutions based on starting Sb_2Te_3 and IT-Ag_2Te compounds below 633 K.[41–43] The decomposition process was additionally confirmed by temperature-dependent X-ray diffraction analysis,[44] and electrochemical measurements.[45] The homogeneity range of the $Ag_{1-x}Sb_{1+x}Te_{2+x}$ phase varies with temperature from 35 to 45 mol% Sb_2Te_3. Recent works are devoted to the search for optimal compositions of this nonstoichiometric phase, which exhibits a high thermoelectric figure of merit.[46,47] The eutectic of the Ag_2Te-Sb_2Te_3 system crystallizes at 70 mol% Ag_2Te and 817 K.[38]

The phase diagram of the PbTe–Sb_2Te_3 boundary system reported in,[48] was characterized by formation only ternary compound $Pb_2Sb_6Te_{11}$, at approximately the eutectic composition on peritectic reaction at 860 K. Shelimova et al.,[49] showed formation in this system also $PbSb_2Te_4$ and $PbSb_4Te_7$ compounds with a layered structure. However, further studies on this system,[50,51] have not confirmed the last compounds. These studies indicated the formation of only the $Pb_2Sb_6Te_{11}$ metastable ternary compound with a 7-layer rhombohedral structure. This metastable phase is stable at high temperatures and decomposes on cooling into PbTe and Sb_2Te_3. However, solidification processing always yields the $Pb_2Sb_6Te_{11}$ phase as a constituent phase observable at room temperature.[50,51] There is an eutectic reaction between $Pb_2Sb_6Te_{11}$ and Sb_2Te_3 at 855 K.[48]

3. Experimental Part

3. 1. Synthesis

All starting compounds Ag_2Te, PbTe, and Sb_2Te_3 of the title system were prepared by melting of elements in evacuated (~10^{-3} Pa) silica ampoules at temperatures ~50 K higher than their melting points.[29] High purity simple substances from the Evochem Advanced Materials GMBH Company (Germany) of were used for synthesis: silver in granules (Ag-00047; 99.999%), antimony in granules (Sb-00002; 99.999%), lead in granules (Pb-00005; 99.9995%), tellurium pieces (Te-00005; 99.9999%). Silver telluride Ag_2Te was additionally annealed at 1200 K for 3 hours and

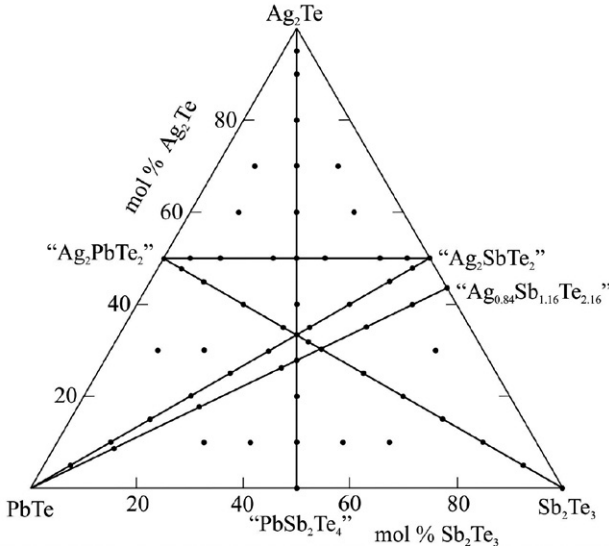

Fig. 1. Studied isopleth sections (*lines*) and alloys (*points*) of the Ag_2Te-PbTe-Sb_2Te_3 system

then was quenched with cold water in order to obtain a homogeneous stoichiometric composition. All starting compounds have been identified using differential thermal analysis and powder X-ray diffraction techniques.

More than sixty alloys of the Ag_2Te-PbTe-Sb_2Te_3 system (Fig. 1) were prepared from the pre-synthesized initial compounds also by vacuum alloying. Considering that the non-stoichiometric phase $Ag_{1-x}Sb_{1+x}Te_{2+x}$ decomposes upon cooling, 2 series of PbTe-"$AgSbTe_2$" and PbTe-"$Ag_{0.84}Sb_{1.16}Te_{2.16}$" alloys with the same compositions were prepared. Alloys from the first series were slowly cooled to 750 K after alloying and then annealed at this temperature for about 700 hours. Alloys from the second series were quenched in cold water after alloying and then also annealed at 750 K (700 h). All alloys after annealing were cooled to room temperature in the off-furnace mode.

3. 2. Analysis

Differential thermal analysis (DTA) and powder X-ray diffraction (PXRD) techniques were employed to analyze both starting compounds and alloys. Thermal analysis of the equilibrated alloys was carried out using a NETZSCH 404 F1 Pegasus system. The DTA measurement was performed between room temperature and ~1300 K with a heating and cooling rate of 10 K min^{-1} under the inert gas (Ar) flow. Temperatures of thermal effects were taken mainly from the heating curves. NETZSCH Proteus Software was used for the evaluation of the DTA data. The PXRD analysis was performed on a Bruker D8 ADVANCE diffractometer, with $CuKa_1$ radiation. PXRD patterns were indexed by using TopasV3.0 software by Bruker.

The electromotive force (EMF) method with glycerol electrolyte,[52] was used for the thermodynamic study of the $(2PbTe)_x(AgSbTe_2)_{1-x}$ solid solutions. Concentration chains of the following type were constructed and their EMF was measured in the temperature range of 300–450 K:

$$(-)\ PbTe\ (s)\ |\ liquid\ electrolyte,\ Pb^{2+}\ |\ (2PbTe)_x(AgSbTe_2)_{1-x}\ (s)\ (+) \qquad (1)$$

Similar electrochemical cells were previously successfully used for thermodynamic studies of several chalcogenide and other inorganic systems.[53–56] Equilibrium alloys $(2PbTe)_x(AgSbTe_2)_{1-x}$ with compositions x = 0.1; 0.15; 0.2; 0.4; 0.6; 0.8 were synthesized by fusing the elementary components in the required ratios into evacuated to ~10^{-2} Pa and sealed quartz ampoules. To maximally approximate the alloys to the equilibrium state, the cast non-homogenized samples obtained by quenching the melts from 1100 K were ground into powder, thoroughly mixed, pressed into tablets weighing 0.3–0.5 g and annealed first at 750 K (500 hours), and then at 450 K (200 h.). Synthesized alloys were identified by PXRD.

To prepare electrodes the PbTe (left electrode) and annealed alloys $(2PbTe)_x(AgSbTe_2)_{1-x}$ (right electrodes) were powdered and pressed onto molybdenum current leads in the form of tablets with a diameter of ~0.6 cm and a thickness of ~0.3 cm.

A solution of KCl in glycerol with the addition of $PbCl_2$ was used as the electrolyte. In order to prevent the presence of moisture and oxygen in the electrolyte anhydrous, chemically pure salts were used, as well as glycerin was previously dehydrated and outgassed by pumping at ~ 400 K.

The electrochemical cell described in,[53] was assembled. EMF measurements were carried out in an inert atmosphere using a high-voltage digital voltmeter V7-91. Before starting the measurements, the electrochemical cell was kept at ~350 K for 40–60 h, after which the first equilibrium EMF values were obtained. Subsequent measurements were carried out every 3–4 hours after the establishment of a certain temperature. The EMF values, which, regardless of the direction of the temperature change did not differ from each other at a given temperature by more than 0.2 mV, were considered to be equilibrium.

Results and Discussion

We have constructed the self-consistent phase diagram of the quasi-ternary Ag_2Te-PbTe-Sb_2Te_3 system as well as determined thermodynamic functions of the PbTe-"$AgSbTe_2$" solid solution by the combined analysis of all our experimental results and the data found in the literature on the phase equilibria for the boundary quasibinary systems.

4. 1. The Sections PbTe-"$AgSbTe_2$" and PbTe-"$Ag_{0.84}Sb_{1.16}Te_{2.16}$"

As mentioned above in Experimental Part, two series of alloys were prepared along these sections. Fig. 2 shows heating curves for PbTe-"$AgSbTe_2$" alloys of both series with compositions 60, 80 and 90 mol% PbTe. As can be seen, the melting onset temperatures of the two series of alloys are very different. For samples of the 1st series (red curves) obtained by slow cooling, the melting onset temperatures are significantly (up to 100°) lower than the samples of the 2nd series (blue curves). Increasing the annealing time up to 1000 h did not change the DTA curves of alloys of the 2nd series, whereas for alloys of the 1st series some (~10–20°) rise in the temperatures of the onset of melting was observed.

These results show that the 2nd series samples can be considered practically in equilibrium. Therefore, data from DTA curves of the 2nd series alloys were used to construct the phase diagram of the PbTe-"$AgSbTe_2$" system (Fig. 3). The PbTe-"$AgSbTe_2$" system is characterized by the formation of wide (up to 70 mol%) solid solutions based on PbTe (β-phase), but the system is generally

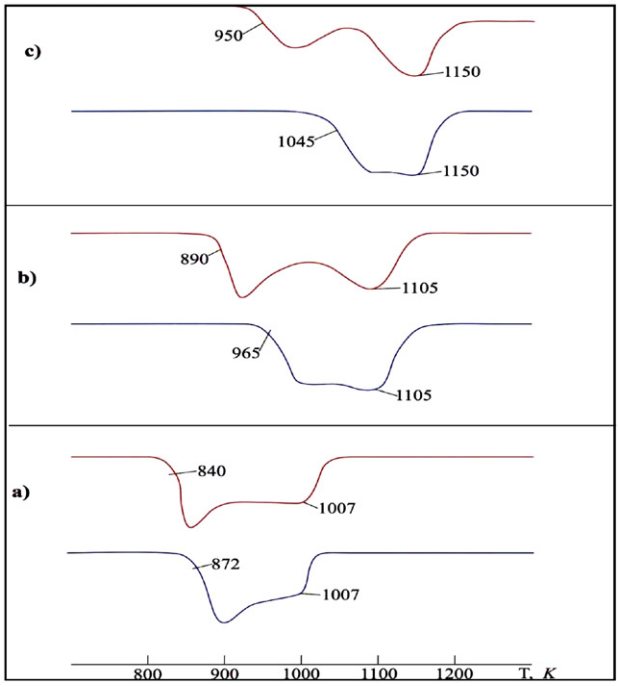

Fig. 2. Fragments of the DTA curves for the PbTe-"$AgSbTe_2$" system alloys with the compositions 60 (**a**), 80 (**b**) and 90 (**c**) mol% PbTe. DTA curves for the samples from the 1st series are red, and from the 2nd series are blue

non-quasi-binary. The reason is the non-individuality of the starting component "$AgSbTe_2$" which is a two-phase alloy $Ag_2Te + Ag_{1-x}Sb_{1+x}Te_{2+x}$.[38,39]

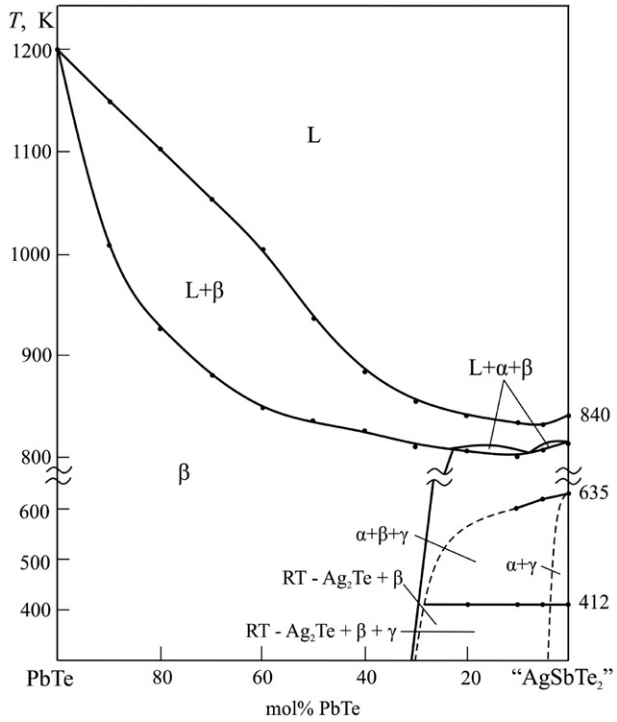

Fig. 3. PbTe-"$AgSbTe_2$" vertical section of the phase diagram of the Ag_2Te-PbTe-Sb_2Te_3 system

The powder X-ray analysis results confirmed the formation of a wide area (30–100 mol% PbTe) of a solid solution with a cubic structure in the studied section. PbTe-poor alloys are three-phase. For example, Fig. 4 represents a powder X-ray pattern of alloy with composition 20 mol% PbTe and 80 mol% "$AgSbTe_2$". As can be seen from Fig. 4 the PXRD pattern of this alloy consists of a set of reflection lines of the RT-Ag_2Te, β-phase, and γ-phase based on Sb_2Te_3.

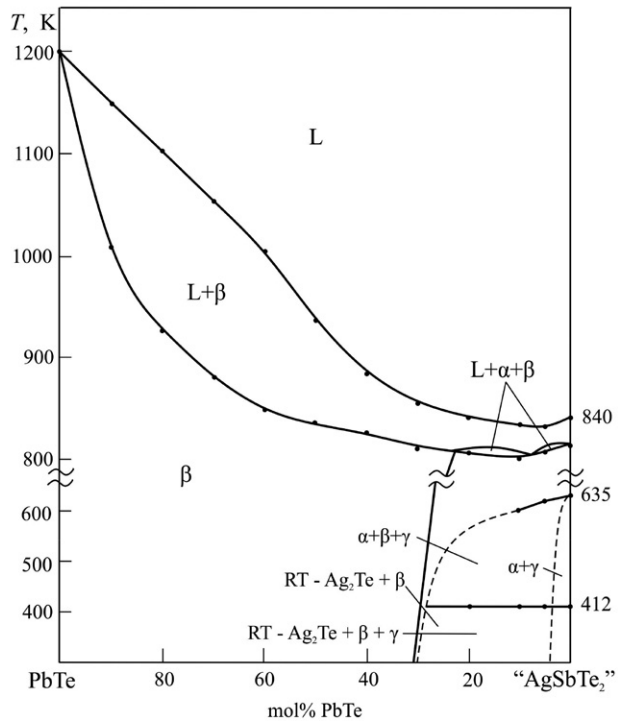

Fig. 4. PXRD patterns and phase composition for alloy with composion 20 mol% PbTe-80 mol% "$AgSbTe_2$"

A characteristic feature of the PbTe-"$AgSbTe_2$" system is a very large temperature range of crystallization (melting) of the β-phase (up to 150°). For this reason, slow cooling of melts leads to strong segregation and inhomogeneity of solid solutions in composition, which makes it difficult to achieve an equilibrium state of the samples. Inhomogeneity of solid solutions in composition in the 1st series alloys is demonstrated by a powder X-ray patterns of an alloy with a composition of 70 mol% PbTe (Fig. 5 a, b). As can be seen, X-ray patterns of samples of this alloy, obtained in two various ways, differ sharply. The sample from the 1st series has very diffuse reflection peaks, while the alloy from the 2nd series has a very high-quality X-ray pattern showing much smoother peaks with minimum noise.

The phase equilibria along the 2PbTe-"$Ag_{0.84}Sb_{1.16}Te_{2.16}$" section (Fig. 6) is qualitatively similar to the PbTe-"$AgSbTe_2$" section. The system is non-quasibinary due to the peritectic melting of the "$Ag_{0.84}Sb_{1.16}Te_{2.16}$"

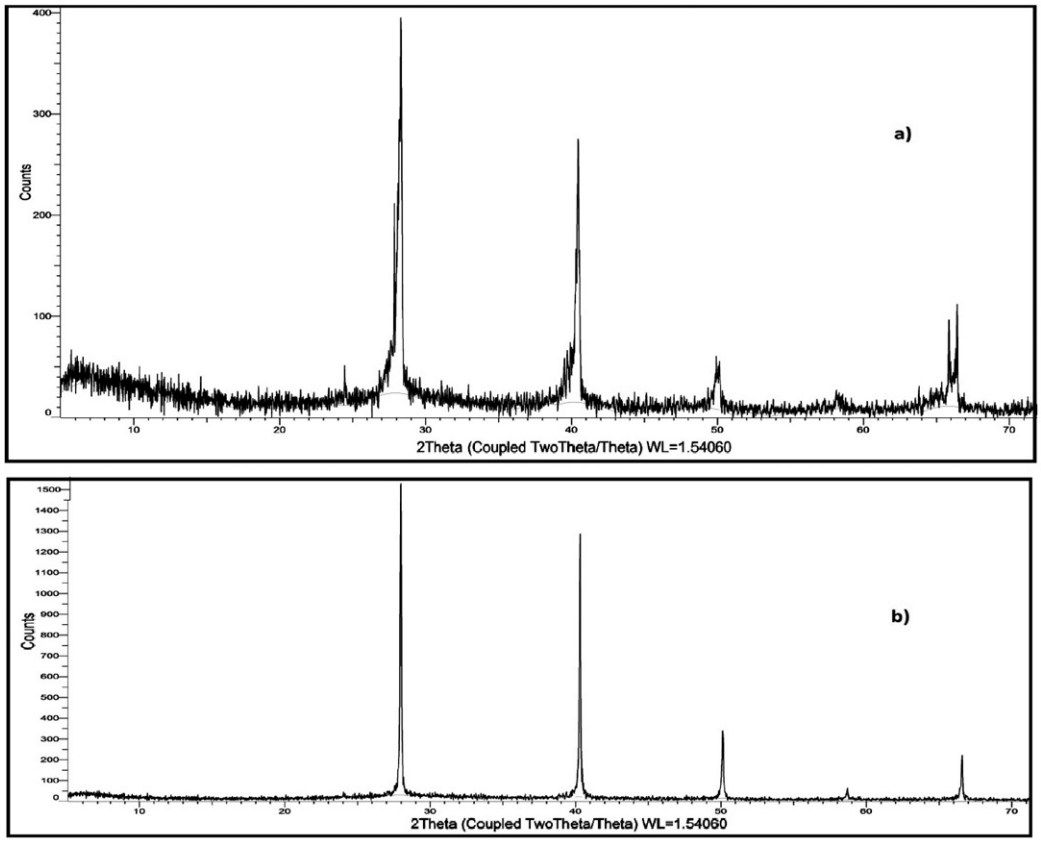

Fig. 5. Powder X-ray patterns of alloy with composition of 70 mol% PbTe: **a)** a sample from the 1st series; **b)** a sample from the 2nd series

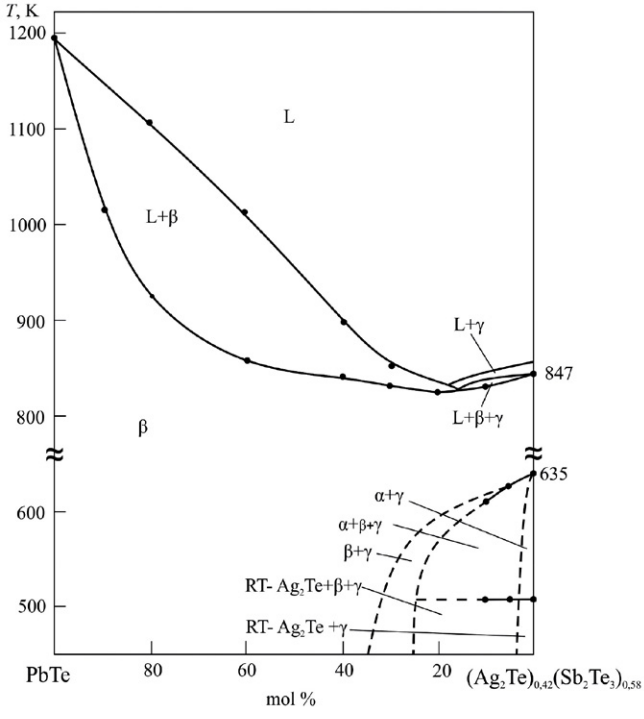

Fig. 6. 2PbTe-"$Ag_{0.84}Sb_{1.16}Te_{2.16}$" vertical section of the phase diagram of the Ag_2Te-PbTe-Sb_2Te_3 system

phase and its decay into Ag_2Te + Sb_2Te_3 below 635 K. This, in turn, leads to the decomposition of β-solid solutions formed in this section in the 0–40 mol% PbTe composition range and, as a result, the α + β + γ, β + γ, α + γ, etc. fields are formed in the system (α-phase is a solid solution based on an IT-Ag_2Te).

Using TopasV3.0 software the lattice parameters of the β-phase were calculated (Table 1) and the concentration dependence of these parameters was plotted (Fig. 7). As can be seen from Fig. 7, the lattice parameters are a linear function of the composition. An insignificant positive deviation of this dependence on the Vegard law is probably caused by elastic deformation of the β-phase'

Table 1. Crystallographic parameters of the b-solid solutions for the 2PbSe-"$Ag_{0.84}Sb_{1.16}Te_{2.16}$"system

Composition, *mol%* $Ag_{0.84}Sb_{1.16}Te_{2.16}$	**Cubic lattice parameter; *a, nm***
0 (PbTe)	0.6463(7)
20	0.6401(7)
40	0.6326(6)
60	0.6252(7)
80	0.6173(3)
100 ($Ag_{0.84}Sb_{1.16}Te_{2.16}$)	0.6077(8)

crystal lattice, due to the large difference in the crystal radius of antimony (0,09 nm) compared to silver (0.129 nm) and lead (0.133 nm). Crystal radii data were taken from.[57]

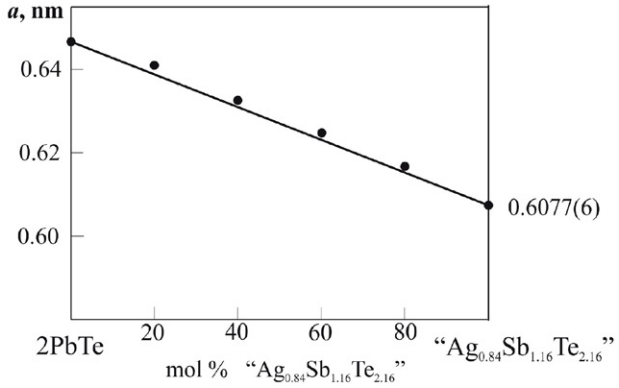

Fig. 7. Concentration dependence of cubic lattice parameter for β-phase along the 2PbTe-"$Ag_{0.84}Sb_{1.16}Te_{2.16}$" section

4. 2. Solid-Phase Equilibria

The isothermal sections at 750 K and 300 K of the phase diagram of the Ag_2Te-PbTe-Sb_2Te_3 system have been constructed.

The isothermal sections at 750 K. A homogeneity range of the intermediate phase $Ag_{1-x}Sb_{1+x}Te_{2+x}$ along PbTe-Sb_2Te_3 section is 40–44 mol% Sb_2Te_3 at 750 K.[38] A wide (up to 8 mol%) continuous band of β-solid solution is formed in the Ag_2Te-PbTe-Sb_2Te_3 system at 750 K (Fig. 8a). The width of a β-solid solutions is 3–4 mol% in the Ag_2Te-Sb_2Te_3 section and expands up to 7–8 mol% with a change in composition towards PbTe. The PbTe-"$Ag_{0.84}Sb_{1.16}Te_{2.16}$" section is completely in the homogeneity area of the β-phase. The PbTe-"$AgSbTe_2$" section in the composition range of 25–100 mol% PbTe passes through the β-phase homogeneity area, and at <25 mol% PbTe passes into the two-phase region α + β. The β-phase forms connode lines with α-phase and γ-phase.

The isothermal sections at 300 K (Fig. 8b). The decomposition of the $Ag_{1-x}Sb_{1+x}Te_{2+x}$ intermediate phase below 635 K leads to partial decomposition of the β-phase in the composition range of <25 mol% PbTe and the following heterogeneous regions are formed: RT-Ag_2Te + β + γ and RT-Ag_2Te + γ.

The location and borders of phase areas on the solid-phase equilibrium diagrams (Fig. 8a, b) were established by using the PXRD technique (for example, powder X-ray pattern of the alloy #1 from Fig. 8b is presented in Fig. 4) and confirmed by the DTA, as well as by the EMF technique (*see sections 4.5*).

4. 3. The Liquidus Surface Projection

The liquidus surface of the Ag_2Te-PbTe-Sb_2Te_3 system consists of 4 fields corresponding to primary crystallization of the α-, β- and γ- phases, as well as ternary compound $Pb_2Sb_6Te_{11}$ (Fig. 9). The α-phase primary crystallization area is separated from the α′-phase based on HT-Ag_2Te by the dashed line. Largest crystallization field in the system belongs to β-phase (field 2 in Fig. 9). This region is divided into 2 parts by the curve M_1M_2 connecting the minimum points of M_1 and M_2. The primary crystallization area of the ternary $Pb_2Sb_6Te_{11}$ compound is very small (field 4 in Fig. 9). Transitional equilibrium *U* limits the extent of this area inside the concentration triangle. This is in good agreement with data,[50,51] on a narrow temperature range for the existence of compound $Pb_2Sb_6Te_{11}$.

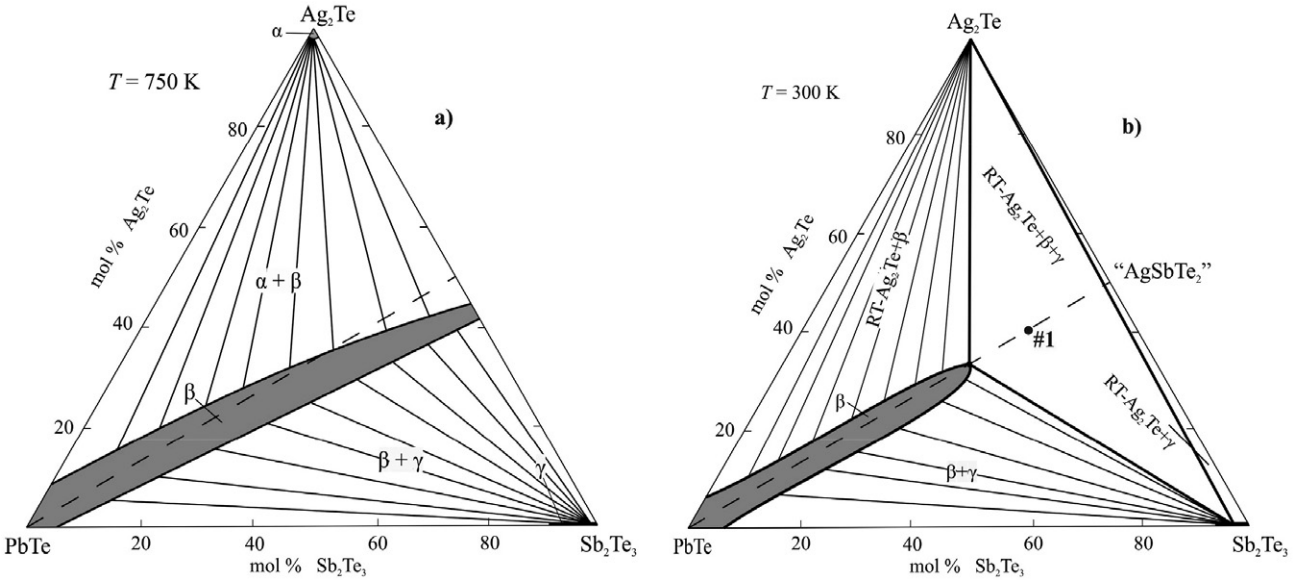

Fig. 8. (a) 750 K and (b) 300 K isothermal sections of the phase diagram of the Ag_2Te-PbTe-Sb_2Te_3 system

Table 2. Nonvariant and monovariant equilibria in the Ag_2Te-PbTe-Sb_2Te_3 system

Point or curve in Fig. 9	Equilibrium	Composition, mol% Ag_2Te	Sb_2Te_3	T, K
P_1	$L + \beta \leftrightarrow Pb_2Sb_6Te_{11}$	–	62	860
P_2	$L + \gamma \leftrightarrow Pb_2Sb_6Te_{11}$	48	52	847
e_1	$L \leftrightarrow Pb_2Sb_6Te_{11} + \gamma$	–	66	855
e_2	$L \leftrightarrow \alpha + \beta$	62	–	967
e_3	$L \leftrightarrow \alpha + Ag_{1-x}Sb_{1+x}Te_{2+x}$	70	30	813
U	$L + Pb_2Sb_6Te_{11} \leftrightarrow \beta + \gamma$	11	59	847
M_1	$L + \gamma \leftrightarrow \beta$	42	46	825
M_2	$L \leftrightarrow \alpha + \beta$	68	27	805
P_1U	$L + \beta \leftrightarrow Pb_2Sb_6Te_{11}$			860–847
e_1U	$L \leftrightarrow Pb_2Sb_6Te_{11} + \gamma$			855–847
UK	$L \leftrightarrow \beta + \gamma$			847–830
KM_1	$L + \gamma \leftrightarrow \beta$			830–825
P_2M_1	$L + \gamma \leftrightarrow \beta$			847–825
M_1M_2	$L \leftrightarrow \gamma$			825–805
e_2M_2	$L \leftrightarrow \alpha + \beta$			967–805
e_3M_2	$L \rightarrow \alpha + \beta$			813–805

The primary crystallization fields of the phases are bordered by peritectic (p_1U, p_2M1) and eutectic (e_2M_2, M_2e_3, e_1U, UM_1) curves (Fig. 9). Types and temperatures for all nonvariant and monovariant equilibria in the Ag_2Te-SnTe-Sb_2Te_3 system are listed in Table 2.

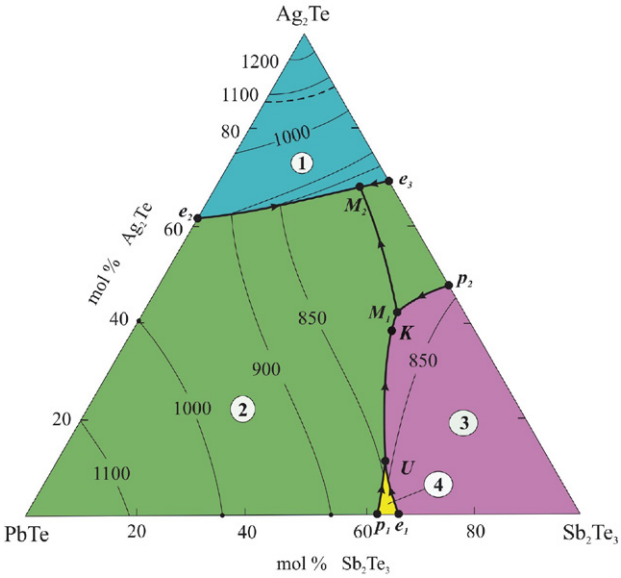

Fig. 9. The liquidus surface projection of the Ag_2Te-PbTe-Sb_2Te_3 system. Primary crystallization fields of phases: 1– α (α′); 2 – β; 3 – γ and 4 – $Pb_2Sb_6Te_{11}$

4. 4. Isopleth Sections

In the context of a liquidus surface projection (Fig.9, Table 2) we consider three isopleth sections which almost completely cover a studied quasi-ternary system.

The section "$AgPb_{0.5}Te$"-"$AgSbTe_2$" (Fig. 10) passes through the region of primary crystallization of the β-phase and intersects the curve M_1M_2. Therefore, a minimum point is observed on the liquidus curve of this section. Below liquidus, crystallization proceeds according to a monovariant eutectic reaction $L \leftrightarrow \alpha + \beta$ (Fig. 10, Table 2, curves e_2M_2, e_3M_2) and, as a result, a two-phase region α + β is formed in the subsolidus. The processes occurring in the system below 635 K and associated with the decomposition of the "$Ag_{1-x}Sb_{1+x}Te_{2+x}$" phase were described above.

The section Ag_2Te-«$PbSb_2Te_4$» (Fig. 11) passes through the areas of primary crystallization of α′, α and β phases. Below the liquidus in the composition range of 0–25 mol% Ag_2Te the univariant processes $L + \beta \leftrightarrow$

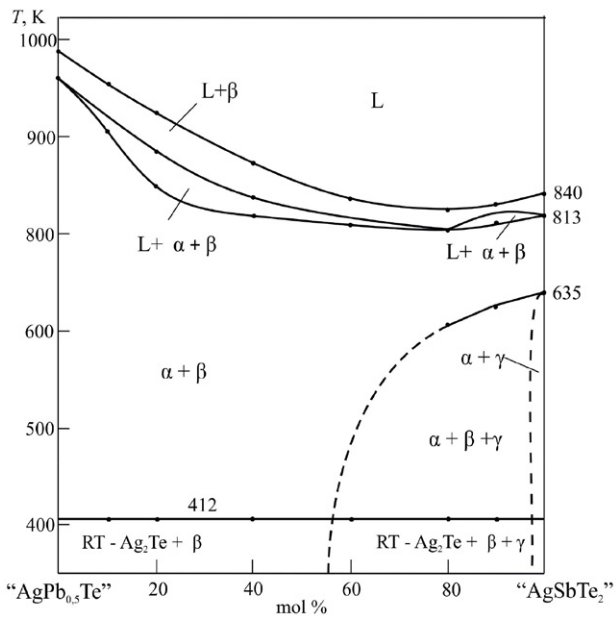

Figure 10. Isopleth section "$AgPb_{0.5}Te$"–"$AgSbTe_2$"

$Pb_2Sb_6Te_{11}$ and L ↔ β + γ occur and the two-phase region β + γ is formed. In the composition range 25–35 mol% Ag_2Te, crystallization continues according to the L ↔ β scheme. In the composition range 25–35 mol% Ag_2Te, as a result of the crystallization process L ↔ α + β a two-phase region RT-Ag_2Te + β is formed in the system due to the α ↔ RT-Ag_2Te phase transition. Note that due to the formation of α′ and α solid solutions, the phase transition temperature α′ ↔ α (~1080 K) increases slightly compared to pure Ag_2Te, which leads to the establishment of the L + α′ ↔ α (*p′*) peritonic equilibrium in the system.

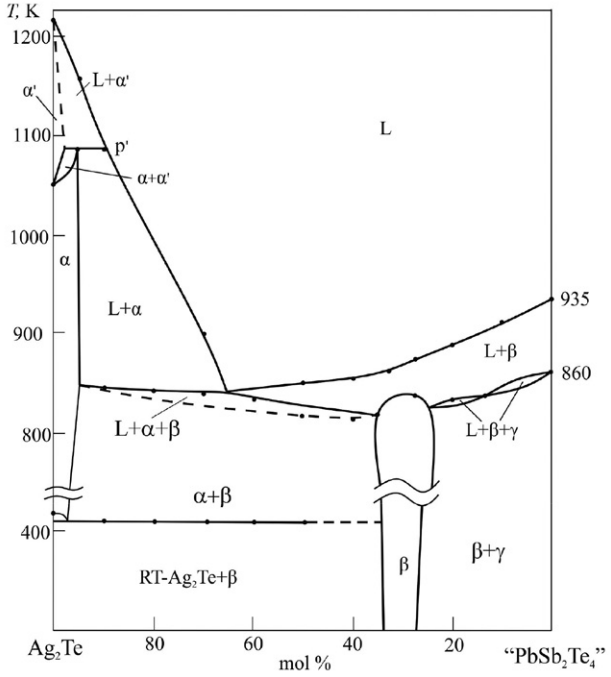

Figure 11. Isopleth section Ag_2Te-«$PbSb_2Te_4$»

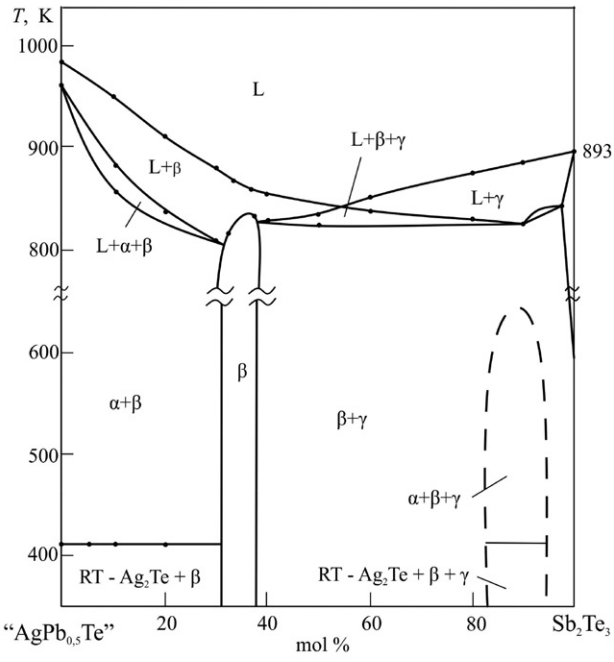

Figure 12. Isopleth section "$AgPb_{0.5}Te$"– Sb_2Te_3

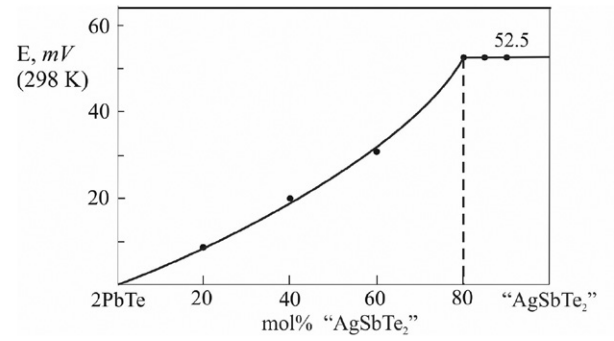

Figure 13. Concentration dependence of the EMF of chains of type (1) at 298 K for the 2PbTe–"$AgSbTe_2$" alloys

The section "$AgPb_{0.5}Te$"-Sb_2Te_3 (Fig. 12) passes through the regions of primary crystallization of β and γ phases. Further, the crystallization process continues according to the monovariant reactions L ↔ α + β (0–30 mol% Sb2Te3), L ↔ β + γ (40–90 mol% Sb2Te3) and L + γ ↔ β (90–98 mol% Sb2Te3). In the range of compositions ~30–38 mol% Sb2Te3, crystallization proceeds according to the L ↔ β reaction and ends with the formation of the β-phase.

4. 5. Thermodynamic Properties of the $(2\ PbTe)_{1-x}(AgSbTe_2)_x$ Solid Solution Obtained with EMF Measurements

Measurements of the EMF of the chains of type (1) showed that the EMF values for samples $(2PbTe)_x(AgSbTe_2)_{1-x}$ with compositions x = 0.1, 0.15 and 0.2 are the same, and with further increase of the concentration of PbTe the values of EMF continuously decrease (Fig. 13). This indicates that in this system up to 80 mol.% solid solutions are produced based on PbTe.

Analysis of the temperature dependences of the EMF showed that for all samples they are linear (Fig.14). Therefore, the experimental data were processed by the least-squares method in the approximation of the linear temperature dependence of the EMF. For this purpose, the "Microsoft Office Excel 2010" software was used.

The obtained linear equations are presented in Table 3 in the following form recommended in,[52]:

$$E = a + bT \pm t\left[\left(S_E^2 / n\right) + S_b^2 \cdot (T - \bar{T})^2\right]^{1/2} \qquad (2)$$

Here *n* is the number of pairs of values of E and T; S_E and S_b are the dispersions of individual measurements of EMF and coefficient b, respectively; $\bar{T}$ is average absolute temperature, *t* is Student's test. With a confidence level of

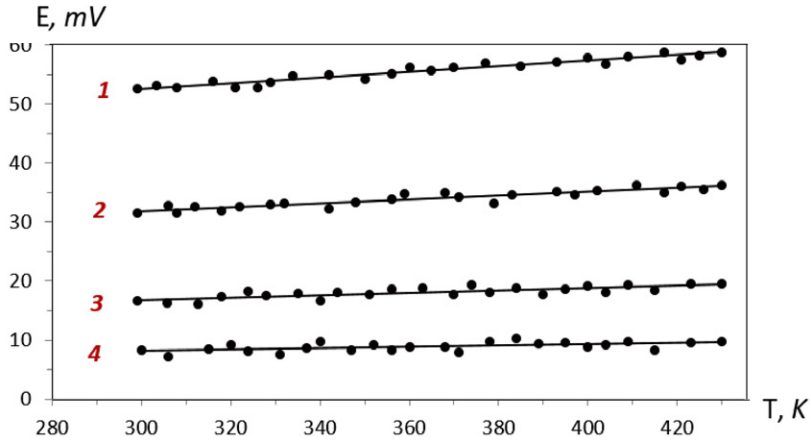

Figure14. Temperature dependences of the EMF of chains of type (1) for the 2PbTe–"$AgSbTe_2$" alloys: ***1*** – $(2PbTe)_{0.2}(AgSbTe_2)_{0.8}$; ***2*** – $(2PbTe)_{0.4}(AgSbTe_2)_{0.6}$; ***3*** – $(2PbTe)_{0.6}(AgSbTe_2)_{0.4}$; ***4*** – $(2PbTe)_{0.8}(AgSbTe_2)_{0.2}$

95% and the number of experimental points $n \geq 20$ the Student's test is $t \geq 2$.

The partial molar functions of PbTe ($\Delta\bar{Z}_{PbTe}$) in alloys at 298.15 K were calculated from the data of Table 3 according to the following relations,[58]:

$$\Delta\overline{G}_{PbTe} = -zFE \tag{3}$$

$$\Delta\overline{S}_{PbTe} = zF\left(\frac{\partial E}{\partial T}\right)_P = zFb \tag{4}$$

$$\Delta\overline{H}_{PbTe} = -zF\left[E + T\left(\frac{\partial E}{\partial T}\right)_P\right] = -zFa \tag{5}$$

Table 3. Temperature dependences of the EMF of cells of type (1) for the $(2PbTe)_x(AgSbTe_2)_{1-x}$ alloys in the 300, 450 K temperature range

Composition	E, mV = a + bT ± t × S_E(T)
$(2PbTe)_{0.2}(AgSbTe_2)_{0.8}$	$38.2+0.048T\pm 2\left[\frac{1.5}{24}+4.8\cdot10^{-5}(T-363.3)^2\right]^{\frac{1}{2}}$
$(2PbTe)_{0.4}(AgSbTe_2)_{0.6}$	$23.6+0.027T\pm 2\left[\frac{1.8}{24}+5.4\cdot10^{-5}(T-362.6)^2\right]^{\frac{1}{2}}$
$(2PbTe)_{0.6}(AgSbTe_2)_{0.4}$	$12.2+0.016T\pm 2\left[\frac{1.1}{24}+3.5\cdot10^{-5}(T-363.6)^2\right]^{\frac{1}{2}}$
$(2PbTe)_{0.8}(AgSbTe_2)_{0.2}$	$5.8+0.009T\pm 2\left[\frac{1.2}{24}+3.7\cdot10^{-5}(T-361.7)^2\right]^{\frac{1}{2}}$

and listed in Table 4. As can be seen from Fig. 15, all these functions are continuous functions of the composition in the field $x \geq 0.2$.

The partial molar functions of PbTe are the difference between the partial molar values of lead in $(2PbTe)_x(AgSbTe_2)_{1-x}$ solid solutions ($\Delta\bar{Z}_{Pb}$) and in pure PbTe:

$$\Delta\overline{Z}_{PbTe} = \Delta\overline{Z}_{Pb} - \Delta\overline{Z}'_{Pb} \tag{6}$$

где $Z \equiv G$ (или H).

PbTe is the only compound of the Pb-Te system and

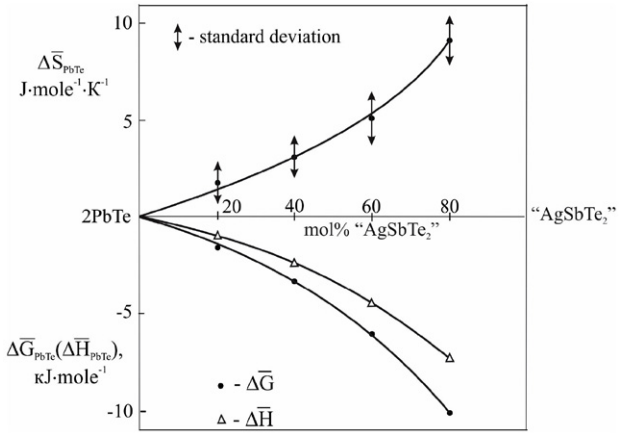

Figure 15. Concentration dependences of partial thermodynamic functions of PbTe in the 2PbTe-"$AgSbTe_2$" solid solutions at 298 K.

Table 4. Relative partial thermodynamic functions of PbTe in the 2PbTe–$AgSbTe_2$ alloys at 298 K

Composition	$-\Delta\bar{G}_{PbTe}$ $\kappa J \times mole^{-1}$	$-\Delta\bar{H}_{PbTe}$ $\kappa J \times mole^{-1}$	$-\Delta\bar{S}_{PbTe}$ $J \times K^{-1} \times mole^{-1}$
$(2PbTe)_{0.2}(AgSbTe_2)_{0.8}$	10,13±0.20	7,37±0.97	9,26±2,67
$(2PbTe)_{0.4}(AgSbTe_2)_{0.6}$	6,11±0.21	4,56±1,03	5,21±2,84
$(2PbTe)_{0.6}(AgSbTe_2)_{0.4}$	3,27±0.17	2,35±0.83	3,09±2,28
$(2PbTe)_{0.8}(AgSbTe_2)_{0.2}$	1,64±0.18	1.12±0.85	1,74±2,34

has an almost constant stoichiometric composition.[34] According to,[58] in such cases:

$$\Delta\overline{Z}'_{Pb} = \Delta_f Z^0(PbTe) \quad (7)$$

Considering relations (6) and (7), the partial molar functions of lead in solid solutions $(2PbTe)_x(AgSbTe_2)_{1-x}$ can be calculated from the relation:

$$\Delta\overline{Z}_{Pb} = \Delta\overline{Z}_{PbTe} + \Delta_f Z^0(PbTe) \quad (8)$$

The values obtained by the relation (8) are presented in Table 5.

The calculation of standard thermodynamic functions of the formation of a solid solution of the limiting composition $(2PbTe)_{0.2}(AgSbTe_2)_{0.8}$, which is in equilibrium with Ag_2Te and Sb_2Te_3, was performed using the following potential-forming reaction:

$$PbTe + Ag_2Te + Sb_2Te_3 = 2.5\ (2PbTe)_{0.2}(AgSbTe_2)_{0.8}.$$

According to this reaction, the standard Gibbs free energy of formation and the enthalpy of formation $(2PbTe)_{0.2}(AgSbTe_2)_{0.8}$ can be calculated by the relation:

$$\Delta_f Z^0[(2PbTe)_{0.2}(AgSbTe_2)_{0.8}] = 0.4\Delta\overline{Z}_{PbTe} + 0.4\Delta_f Z^0(PbTe) + 0.4\Delta_f Z^0(Ag_2Te) + 0.4\Delta_f Z^0(Sb_2Te_3) \quad (9),$$

and entropy can be calculated from the relation:

$$S^0[(2PbTe)_{0.2}(AgSbTe_2)_{0.8}] = 0.4S_{PbTe} + 0.4S^0(PbTe) + 0.4S^0(Ag_2Te) + 0.4S^0(Sb_2Te_3) \quad (10).$$

Standard integral thermodynamic functions of the formation of solid solutions with compositions x = 0.4; 0.6 and 0.8 were calculated by integrating the Gibbs-Duhem equation:

$$\Delta_f Z^0[(2PbTe)_x(AgSbTe_2)_{1-x}] = 2(1-x) \int_{0.2}^{x} \frac{\Delta\overline{Z}_{PbTe}}{(1-x)^2}dx + x\Delta_f Z^0[(2PbTe)_{0.2}(AgSbTe_2)_{0.8}] \quad (11)$$

Errors were found by the method of accumulation of errors. The first term on the right side of equation (11) was determined by integrating by means of the trapezoid method using the "Microsoft Office Excel 2010" software.

Literature data on corresponding standard integral thermodynamic functions of the Ag_2Te, PbTe and Sb_2Te_3 compounds in addition to own experimental results (Table 4), were used at calculations of equations (9) and (10) (Table 6).

The values of standard enthalpies of formation and entropies for PbTe and Sb_2Te_3 were taken from Ref.[58] For the Ag_2Te compound, the data of,[59] obtained by the EMF

Table 5. Relative partial thermodynamic functions of lead in the $2PbTe–AgSbTe_2$ alloys at 298 K

Composition	$-\Delta\bar{G}_{Pb}$ *κJ mole⁻¹*	$-\Delta\bar{H}_{Pb}$ *κJ mole⁻¹*	$-\Delta\bar{S}_{Pb}$ *J × K⁻¹ mole⁻¹*
$(2PbTe)_{0.2}(AgSbTe_2)_{0.8}$	77,43±1,70	75,97±1,57	4,90±4,77
$(2PbTe)_{0.4}(AgSbTe_2)_{0.6}$	73,41±1,71	73,16±1,63	0,84±4,94
$(2PbTe)_{0.6}(AgSbTe_2)_{0.4}$	70,57±1,67	70,95±1,43	–1,74±4,38
$(2PbTe)_{0.8}(AgSbTe_2)_{0.2}$	68,94±1,68	69,72±1,45	–2,62±4,44

Table 6. Standard integral thermodynamic functions of the $(2PbTe)_{1-x}(AgSbTe_2)_x$ solid solutions

Phase	$-\Delta_f G°$ (298 *K*) *κJ mole⁻¹*	$-\Delta_f H°$ (298 *K*) *κJ mole⁻¹*	S° (298 *K*), *J × K⁻¹ mole⁻¹*
PbTe,[58]	67.3±1.5	68.6±0.6	110.0±2.1
Sb_2Te_3,[58]	56.9±1.0	56.5±0.4	246.4±2.1
Ag_2Te,[59]	40.2±0.3	35.0±0.5	152.0±2.0
$(2PbTe)_{0,9}(AgSbTe_2)_{0,1}$	128.5±2.8	130.0±1.2	217.6±4.1
$(2PbTe)_{0,8}(AgSbTe_2)_{0,2}$	119.0±2.5	121.9±1.1	218.4±3.9
	122.2±2.9*	**122.3±2.5***	**220.0±3.5***
$(2PbTe)_{0,6}(AgSbTe_2)_{0,4}$	104.3±2.0	104.2±0.9	213.7±3.4
	106.4±2.3*	**105.2±2.0***	**216.1±3.5***
$(2PbTe)_{0,4}(AgSbTe_2)_{0,6}$	86.3±1.6	85.4±0.9	208.2±3.5
	89.1±1.8*	**86.8±1.5***	**211.5±3.8***
$(2PbTe)_{0,2}(AgSbTe_2)_{0,8}$	67.3±1.1	66.0±0.7	202.2±3.0
	69.8±1.2*	**67.0±0.9***	**204.9±3.7***

* these values are obtained by the EMF method with solid electrolyte,[61]

The values of standard enthalpies of formation and entropies for PbTe and Sb_2Te_3 were taken from Ref.[58] For the Ag_2Te compound, the data of,[59] obtained by the EMF

method were used. Using the EMF method with solid Ag^+ conducting electrolyte,[60] thermodynamic data for investigated solid solutions previously were obtained in,[61] and also are listed in Table 6. As can be seen, the results obtained by two modifications of the EMF method, agree within the margin of inaccuracies.

5. Conclusıon

A complete description of the phase equilibria in the quasi-ternary Ag_2Te-PbTe-Sb_2Te_3 system, including 750 and 300 K isothermal sections and five isopleth sections of the phase diagram, as well as liquidus surface projection, were obtained. This system characterized by the formation of a wide continuous high-temperature solid solution (β-phase) with a cubic structure between PbTe and "$Ag_{1-x}Sb_{1+x}Te_{2+x}$" intermediate phase. Below 635 K, a solid-state decomposition of the β-phase occurs and subsequently the formation of the α- and γ-phases based correspondingly on IT-Ag_2Te and Sb_2Te_3 were observed.

The formation of a wide (up to 80 mol%) region of solid solutions based on PbTe along the 2PbTe-"$AgSbTe_2$" section was confirmed by measuring EMF of the concentration chains concerning to the PbTe electrode. A new mutually agreed complex of data on standard partial thermodynamic functions of PbTe and lead, as well as integral thermodynamic functions of β-solid solutions along the above section was obtained. This data is in agreement with the results obtained earlier by the EMF method with solid Ag^+ conductive electrolyte.[61]

The presented results can be used for the design of new LAST alloys, which are of great interest as thermoelectric materials.

6. References

1. Applications of Chalcogenides: S, Se, and Te / Ed. Ahluwalia G. K, **2016**, Cham.: Springer, 461p.
2. A. V. Kolobov, J. Tominaga, Chalcogenides, **2012**, Springer.
3. M. -R. Gao, Y. -F. Xu, J. Jiang, S. -H. Yu, *Chemical Society Reviews*, **2013**, *42(7),* 2986. **DOI:**10.1007/978-3-642-28705-3
4. I. Riess, *Solid State Ion.*, **2003**, *157*, 1–17. **DOI:**10.1039/c2cs35310e
5. H. Wada, M. Ishii, M. Onoda, M. Tansho, A. Sato, *Solid State Ionics*, **1996**, *86–88*, 159–163. **DOI:**10.1016/S0167-2738(02)00182-0
6. C. Gayner, K. K. Kar, *Progress in Materials Science*, **2016**, *83*, 330–382. **DOI:**10.1016/j.pmatsci. 2016.07.002
7. A. V. Shevelkov, *Russ. Chem. Rev.*, **2008**, *77 (1),* 1–19. **DOI:**10.1070/RC2008v077n01ABEH003746
8. F. Tesfaye, M. Moroz, *Journal of Electronic Research and Application*, **2018**, *2 (2),* 28–41. **DOI:**10.26689/jera.v2i2.337
9. G. Tan, F. Shi, H. Sun, L. -D. Zhao, C. Uher, V. P. Dravid, M. G. Kanatzidis, *J. Mater. Chem. A*, **2014**, *2*, 20849–20854. **DOI:**10.1039/C4TA05530F
10. A. Dahshan, H. H. Hegazy, K. A. Aly, P. Sharma, *Physica B: Condensed Matter*, **2017**, *526*, 117–121. **DOI:**10.1016/j. physb. 2017.09.097
11. D. Niesner, S. Otto, V. Hermann, Th. Fauster, T. V. Menshchikova, S. V. Eremeev, Z. S. Aliev, I. R. Amiraslanov, P. M. Echenique, M. B. Babanly, E. V. Chulkov, *Physical Review B*, **2014**, *89*, 081404–081404–5. **DOI:**10.1103/PhysRevB.89.081404
12. M. Papagno, S. Eremeev, J. Fujii, Z. Aliev, M. B. Babanly, S. Mahatha, I. Vobornik, N. Mam, D. Pacile, E. Chulkov, *ACS Nano*, **2016**, *10 (3)*, 3518–3524. **DOI:**10.1021/acsnano.5b07750
13. T. Okuda, T. Maegawa, M. Ye, K. Shirai, T. Warashina, K. Miyamoto, K. Kuroda, M. Arita, Z. S. Aliev, I. R. Amiraslanov, M. B. Babanly, E. V. Chulkov, S. V. Eremeev, A. Kimura, H. Namatame, M. Taniguchi, *Phys. Rev. Lett. (American Phys. Soc.),* **2013**, *111*, 205803–5. **DOI:**10.1103/PhysRevLett.111.206803
14. D. Pacile, S. V. Eremeev, M. Caputo, M. Pisarra, O. De Luca, I. Grimaldi, J. Fujii, Z. S. Aliev, M. B. Babanly, I. Vobornik, R. G. Agostino, A. Goldoni, E. V. Chulkov, M. Papagno. *Physica status solidi (RRL) – Rapid Research Letters,* **2018**, *12 (12)*, 1800341–8. **DOI:**10.1002/pssr.201800341
15. I. Horichok, R. Ahiska, D. Freik, L. Nykyruy, S. Mudry, O. Matkivskiy, T. Semko, *Journal of Electronic Materials,* **2016**, *45(3)*, 1576–1583. **DOI:**10.1007/s11664-015-4122-9
16. J. Liu, L. M. Peng, *Applied Mechanics and Materials*, **2014**, *456*, 490–493. **DOI:**10.4028/www.scientific.net/AMM. 456. 490
17. Y. Chen, B. He, T. J. Zhu, X. B. Zhao, *Journal of Physics D: Applied Physics,* 2012, *45(11),* 115302. **DOI:**10.1088/0022-3727/45/11/115302
18. B. Kusz, T. Miruszewski, B. Bochentyn, M. Łapiński, J. Karczewski, *Journal of Electronic Materials,* **2016**, 45(2), 1085–1093. **DOI:**10.1007/s11664-015-4251-1
19. A. Kumar, P. A. Vermeulen, B. J. Kooi, J. Rao, L. van Eijck, S. Schwarzmüller, O. Oeckler, G. R. Blake. *Inorganic Chemistry,* **2017**, *56(24),* 15091–15100. **DOI:**10.1021/acs.inorgchem.7b02433
20. M. B. Babanly, E. V. Chulkov, Z. S. Aliev, A. V. Shevel'kov, I. R. Amiraslanov, *Russ. J. Inorg. Chem.,* **2017**, *62(13)*, 1703–1729. **DOI:**10.1134/S0036023617130034
21. P. Villars, A. Prince, H. Okamoto, Handbook of Ternary Alloy Phase Diagrams (10 volume set). American Technical Publishers, **1995**, 15000 p.
22. G. Gottstein Physical Foundations of Material Science, Springer, **2004**, 502 p. **DOI:**10.1007/978-3-662-09291-0
23. F. M. Mammadov, I. R. Amiraslanov, Y. A . Aliyeva, S. S. Ragimov, L. F. Mashadiyeva, M. B. Babanly, *Acta Chim. Slov.,* **2019**, *66*, 1–7. **DOI:**10.17344/acsi.2019.4988
24. S. Z. Imamaliyeva, G. I. Alakbarzade, M. A. Mahmudova, I. R. Amiraslanov, M. B. Babanly, *Acta Chim. Slov.,* **2018,** *65,* 365–371. **DOI:**10.17344/acsi.2017.4053
25. D. M. Babanly, I. I. Aliev, K. N. Babanly, Yu. A. Yusibov, *Russ. J. Inorg. Chem.,* **2011**, *56 (9),* 1472–1477.

DOI:10.1134/S0036023611090038
26. L. F. Mashadiyeva, J. O. Kevser, I. I. Aliev, Y. A. Yusibov, D. B. Taghiyev, Z. S. Aliev, M. B. Babanlı, *J. Alloys . Compd*., **2017**, *724,* 641–648. **DOI:**10.1016/j.jallcom.2017.06.338
27. L. F. Mashadiyeva, J. O. Kevser, I. I. Aliev, Y. A. Yusibov, D. B. Taghiyev, Z. S. Aliev, M. B. Babanlı, *Phase equilibria and diffusion*, **2017**, *38 (5)*, 603–614. **DOI:**10.1007/s11669-017-0583-2
28. L. F. Mashadieva, Yu. A. Yusibov, Dzh. Kevser, M. B. Babanly, *Russ. J. Phys. Chem. A,* **2017**, *91 (9)*, 1642–1646. **DOI:**10.1134/S0036024417090187
29. T. B. Massalski (Ed.), Binary Alloy Phase Diagrams, second ed., ASM International, Materials Park, Ohio, **1990**, p. 3589.
30. A. Lee, A., J. L. de Boer, *Acta Cryst. C,* **1993**, *49*, 1444–1446. **DOI:**10.1107/S0108270193003294
31. J. Schneider, H. Schulz, *Z. Kristallogr.,* **1993**, *203*, 1–15. **DOI:**10.1524/zkri. 1993. 203. Part-1. 1
32. A. J. Frueh, *Am. Mineral.,* **1961**, *46*, p. 654-660.
33. P. B. Pereira, I. Sergueev, S. Gorsse, J. Dadda, E. Müller, R. P. Hermann, *Physica Status Solidi (b)*, **2012**, *250(7)*, 1300–1307. **DOI:**10.1002/pssb.201248412
34. T. L. Anderson, H. B. Krause, *Acta Crystallogr. B,* **1974**, *30*, 1307–1310. **DOI:**10.1107/S0567740874004729
35. F. Wald, *J. Less Common. Met.,* **1967**, *13 (6)*, 579–590. **DOI:**10.1016/0022-5088(67)90103-8
36. R. Blachnik, B. Gather, *J. Less_Common. Met.,* **1978**, *60 (1)*, 25–32. **DOI:**10.1016/0022-5088(78)90086-3
37. K. Bergum, T. Ikeda, G. Jeffrey-Snyder, *Journal of Solid State Chemistry*, **2011**, *184(9),* p. 2543–2552. **DOI:**10.1016/j.jssc.2011.07.012
38. G. Petzow, G. Effenberg: „Ternary Alloys", Wiley-VCH Verlag, Weinheim, **1988**, 2, p. 554
39. R. M. Marin-Ayral, B. Legendre, G. Brun, B. Liautard, J. C. Tedenac, *Thermochimica Acta*, **1988**, *131*, 37–45. **DOI:**10.1016/0040-6031(88)80055-8
40. S. Geller, J. H. Wernick, *Acta Crystallogr.,* **1959**, *12*, 46. **DOI:**10.1107/S0365110X59000135
41. H. J. Wu, S. W. Chen, *Acta Mater.,* **2011**, *59*, 6463–6472. **DOI:**10.1016/j. actamat. 2011.07.010
42. P. M. Wyzga, K. T. Wojciechowski, *J. Electron. Mater.,* **2016**, *45*, 1548–1554. **DOI:**10.1007/s11664-015-4102-0
43. K. T. Wojciechowski, M. Schmidt, *Phys. Rev. B,* **2009,** *79*, 184202–7. **DOI:**10.1103/PhysRevB.79.184202
44. B. Du, Y. Yan, X. Tang, *J. Electron. Mater.,* **2015**, *44*, 2118–2123. **DOI:**10.1007/s11664-015-3682-z
45. M. Aspiala, P. Taskinen, *J. Chem. Thermodyn.* **2016**, *93*, 261–266. **DOI:**10.1016/j.jct.2015.08.025
46. P. Wyżga, I. Veremchuk, U. Burkhardt, P. Simon, Y. Grin, K. Wojciechowski, *Applied Sciences,* **2018**, *8(1)*, 52–70. **DOI:**10.3390/app8010052
47. H. Matsushita, E. Hagiwara, A. Katsui, *Journal of Materials Science*, **2004**, *39(20),* 6299–6301. **DOI:**10.1023/B:JMSC.0000043599.86325.ba
48. N. K. Abrikosov, E. L. Elagina, M. A. Popova, *Inorg. Mater.,* **1965**, *1*, 1944–1946.
49. L. E. Shelimova, O. G. Karpinskii, T. E. Svechnikova, E. S. Avilov, M. A. Kretova, V. S. Zemskov, *Inorganic Materials,* **2004,** *40(12)*, 1264–1270. **DOI:**10.1007/s10789-005-0007-2
50. T. Ikeda, S. M. Haile, V. A. Ravi, H. Azizgolshani, F. Gascoin, G. J. Snyder, *Acta Mater*., **2007**, *55*, 1227–1239. **DOI:**10.1016/j. actamat. 2006. 09. 036
51. T. Ikeda, J. Synder, *MRS Proceedings*, **2010**, 1267–5. **DOI:**10.1557/PROC-1267-DD06-07
52. A. G. Morachevskiy, G. F. Voronin, V. A. Geyderikh, I. B. Kutsenok, Electrochemical research methods in the thermodynamics of metal systems, "Akademkniga", **2003**, 334 p. (*In Russian*)
53. S. Z. Imamaliyeva, S. S. Musayeva, D. M. Babanly , Y. I. Jafarov, D. B. Tagiyev, M. B. Babanly, *Thermochimica Acta*, **2019**, *679*, 178319–7. **DOI:**10.1016/j.tca.2019.178319
54. D. M. Babanly, L. F. Mashadieva, M. B. Babanly, *Inorganic Materials*, **2017**, *53(5)*, 519–524. **DOI:**10.1134/S002016851705003X
55. M. Rozman, U. Bren, M. Lukšič, R. F. Godec, G. Bokias, A. N. Kalarakis, E. Stathatos, *Electrochimica Acta*, **2018**, *283*, 1105–1114. **DOI:**10.1016/j.electacta. 2018.07.052
56. S. Z. Imamalieva, D. M. Babanly, T. M. Gasanly, D. B. Tagiev, M. B. Babanly. *Russian Journal of Physical Chemistry A,* **2018**, *92(11),* 2111–2117. **DOI:**10.1134/S0036024418110158
57. R. D. Shannon, Revised Effective Ionic Radii and Systematic Studies of Interatomic Distances in Halides and Chalcogenides, Acta Crystallographica, **1976**, A32, p. 751–767 (Digital version: Database of Ionic Radii; **DOI:**10.1107/S0567739476001551
58. Data base of thermal constants of substances (Digital version, In: Yorish V. S., Yungman V. S. (Ed.), **2006**, http://www. chem. msu. ru/cgi-bin/tkv).
59. M. V. Voronin, E. G. Osadchii, E. A. Brichkina, *Physics and Chemistry of Minerals,* **2017**, *44(9),* 639–653. **DOI:**10.1007/s00269-017-0889-y
60. L. F. Mashadieva, Sh. G. Mansimova, Yu. A. Yusibov, M. B. Babanly, *Russian Journal of Electrochemistry,* **2018**, *54 (1)*, 106–111. **DOI:**10.1134/S102319351711009X
61. M. B. Babanly, Y. A. Yusibov, N. B. Babanly, The EMF method with solid-state electrolyte in the thermodynamic investigation of ternary Copper and Silver Chalcogenides. Electromotive force and measurement in several systems. / Ed. Kara S. InTech. Org. 2011. P. 57. **DOI:**10.5772/28934

Povzetek

Raziskovali smo fazna ravnotežja v sistemu Ag_2Te-PbTe-Sb_2Te_3 z metodami diferencialne termične analize, praškovne rentgenske difrakcije in meritvami elektromotorne sile (EMF). Konstruirali smo površinsko projekcijo sistema, izotermalne odseke pri 750 K in 300 K, ter pet vertikalnih odsekov faznega diagram. Določili smo primarna kristalizacijska področja in območja homogenosti faz. Identificirali smo vrsto in temperature različnih nevariantnih in monovariantnih ravnotežij. Značilnost preučevanega sistema je nastanek širokega zveznega pasu visokotemperaturne kubične trdne raztopine (β-faza) med PbTe in $Ag_{1-x}Sb_{1+x}Te_{2+x}$. Na osnovi rezultatov meritev EMF smo izračunali parcialne molarne termodinamske funkcije svinčevega telurida v zlitinah in standardne integralne termodinamske funkcije β-trdnih raztopin vzdolž odseka 2PbTe-«$AgSbTe_2$«.